



1 **Conformational features and ionization states of Lys side chains in a protein**  
2 **revealed by the stereo-array isotope labeling (SAIL) method**

3

4 Mitsuhiro Takeda<sup>1,2</sup>, Yohei Miyanoiri<sup>1,3</sup>, Tsutomu Terauchi<sup>4,5</sup>,  
5 and Masatsune Kainosho<sup>1,5\*</sup>

6

7 <sup>1</sup>Structural Biology Research Center, Graduate School of Science, Nagoya University, Furo-cho,  
8 Chikusa-ku, Nagoya, 464-8602 Japan; <sup>2</sup>Department of Structural BioImaging, Faculty of Life  
9 Sciences, Kumamoto University, 5-1, Oe-honmachi, Chuo-ku, Kumamoto, 862-0973 Japan;  
10 <sup>3</sup>Research Center for State-of-the-Art Functional Protein Analysis, Institute for Protein Research,  
11 Osaka University, 3-2 Yamadaoka, Suita, Osaka, 565-0871 Japan; <sup>4</sup>SAIL Technologies Co., Inc.,  
12 2008-2 Wada, Tama-city, Tokyo, 206-0001 Japan; <sup>5</sup>Graduate School of Science, Tokyo  
13 Metropolitan University, 1-1 Minami-ohsawa, Hachioji, Tokyo, 192-0397 Japan

14

15 \*Correspondence should be addressed to:

16 Masatsune Kainosho, Ph.D.

17 Graduate School of Science, Tokyo Metropolitan University, 1-1 Minami-ohsawa, Hachioji,  
18 Tokyo 192-0397, Japan

19 E.mail: [kainosho@tmu.ac.jp](mailto:kainosho@tmu.ac.jp)

20

21 Dedicated to Professor Robert Kaptein on the occasion of his 80<sup>th</sup> birthday.



22 **Abstract**

23 Although both the *hydrophobic* aliphatic chain and *hydrophilic*  $\zeta$ -amino group of the Lys side  
24 chain presumably contribute to the structures and functions of proteins, the *dual* nature of the Lys  
25 residue has not been fully investigated by NMR spectroscopy, due to the lack of appropriate  
26 methods to acquire comprehensive information on its long consecutive methylene chain. We  
27 describe herein a robust strategy to address the current situation, using various isotope-aided NMR  
28 technologies. The feasibility of our approach is demonstrated for the  $\Delta$ +PHS/V66K variant of  
29 *Staphylococcal* nuclease (SNase), which contains as many as 21 Lys residues, including the  
30 engineered Lys-66 with an unusually low  $pK_a$  of  $\sim 5.6$ . All of the NMR signals for the 21 Lys  
31 residues were sequentially and stereo-specifically assigned by using the stereo-array isotope  
32 labeled Lys (SAIL-Lys),  $[U-^{13}C, ^{15}N; \beta_2, \gamma_2, \delta_2, \epsilon_3-D_4]$ -Lys. The unambiguously assigned NMR  
33 signals for the  $\beta$ -,  $\gamma$ -,  $\delta$ - and  $\epsilon$ -methylene moieties afforded a variety of crucial structural  
34 information, which could not be obtained by other methods. For example, the  $^{13}C^\epsilon$  signals in the  
35 SNase variant, selectively labeled with  $[\epsilon-^{13}C; \epsilon, \epsilon-D_2]$ -Lys, were  $\sim 0.3$  ppm up-field shifted in  $D_2O$ ,  
36 as compared to those in  $H_2O$ , except for Lys-66, which showed a  $\sim 0.2$  ppm up-field shift in  $D_2O$ .  
37 This result indicates that the deuterium-induced up-field shifts of the  $^{13}C^\epsilon$  signals depend on the  
38 ionization states of the  $\zeta$ -amino group; i.e.,  $\sim -0.3$  ppm for  $\Delta\delta^{13}C^\epsilon [N^\zeta D_3^+ - N^\zeta H_3^+]$  and  $\sim -0.2$  ppm  
39 for  $\Delta\delta^{13}C^\epsilon [N^\zeta D_2 - N^\zeta H_2]$ . Since the highly sensitive 1D- $^{13}C$  NMR spectrum of a protein selectively  
40 labeled with  $[\epsilon-^{13}C; \epsilon, \epsilon-D_2]$ -Lys shows extremely narrow, well-dispersed  $^{13}C$  signals, the  
41 deuterium-induced isotope shifts will be a powerful alternative tool to characterize the ionization  
42 states of the Lys  $\zeta$ -amino groups in larger proteins.

43



44

## 45 **1 Introduction**

46 Detailed studies on the structures and dynamics of the Lys residues in a protein have been severely  
47 hampered by the difficulty in gathering comprehensive NMR information on their side chain  
48 moieties. It is especially challenging to establish *unambiguous* stereo-specific assignments for the  
49 prochiral protons in the four consecutive methylene chain, which is the longest aliphatic chain  
50 among the 20 common amino acids. Given the lack of generally applicable strategies to overcome  
51 this obstacle, only a few systematic NMR studies have probed the structural aspects of the Lys  
52 residues. The ionization states of the Lys  $\zeta$ -amino groups also provide important information, as  
53 they are often involved in specific intra- and/or intermolecular molecular recognition processes,  
54 and thus play vital roles in protein functions. Therefore, the side chain moieties of Lys residues are  
55 considered to contribute to maintaining the structure and biological functions of a protein by these  
56 two elements: the *hydrophobic* methylene chain and the *hydrophilic*  $\zeta$ -amino group. To investigate  
57 the *dual* nature of the Lys side chain, we have applied various isotope-aided NMR technologies,  
58 including the stereo-array isotope labeling (SAIL) method (Kainosho et al., 2006).

59 The Lys  $\zeta$ -amino groups, which usually have pK<sub>a</sub> values around 10.5, are protonated (NH<sub>3</sub><sup>+</sup>)  
60 at around neutral pH. However, certain proteins have Lys residues with deprotonated  $\zeta$ -amino  
61 groups even at neutral or acidic pH (Harris and Turner, 2002). In such cases, the pK<sub>a</sub> values of the  
62 Lys  $\zeta$ -amino groups are substantially lowered due to their particular local environments. Since the  
63 Lys  $\zeta$ -NH<sub>2</sub> groups are endowed with significantly different physical chemical properties, as  
64 compared to the  $\zeta$ -NH<sub>3</sub><sup>+</sup>, they can perform specific functions such as Schiff base formation through  
65 nucleophilic attacks on various substrates (Highbarger et al., 1996; Barbas et al., 1997). Although  
66 the ionization states of Lys  $\zeta$ -amino groups in a protein have been characterized by X-ray  
67 crystallography, they may not always be identical to those in solution. The NH<sub>3</sub><sup>+</sup> and NH<sub>2</sub> states  
68 of Lys residues in solution could also be identified by the cross peak patterns in the <sup>1</sup>H-<sup>15</sup>N  
69 correlation NMR spectra, if the hydrogen exchange rates are sufficiently slow, or by the <sup>15</sup>N $\zeta$  and/or  
70 <sup>1</sup>H $\zeta$  chemical shifts (Poon et al., 2006; Iwahara et al., 2007; Takayama et al., 2008). Under  
71 physiological conditions, however, the observations of <sup>1</sup>H-<sup>15</sup>N cross peaks are often hampered due  
72 to the rapid hydrogen exchange rates of the Lys  $\zeta$ -amino groups (Liepinsh et al., 1992; Liepinsh



73 and Otting, 1996; Otting and Wüthrich, 1989; Otting et al., 1991; Segawa et al., 2008). The  
74 ionization states can also be identified by the pH titration profiles for the  $^{13}\text{C}^\epsilon$  and  $^{15}\text{N}^\zeta$  signals of  
75 individual Lys residues (Kesvatera et al., 1996; Damblon et al., 1996; Farmer and Venters, 1996;  
76 Poon et al., 2006; Gao et al., 2006; André et al., 2007). Unfortunately, long-term experiments such  
77 as pH titration are hampered by the stability and solubility issues of a protein over the wide pH  
78 range. Therefore, straightforward and robust alternative methods to identify Lys residues with  
79 distinct ionization states for the  $\zeta$ -amino groups are highly desired.

80 We used a variant of *Staphylococcal* nuclease,  $\Delta$ +PHS/V66K SNase (denoted as the SNase  
81 variant, hereafter), as the model protein (Stites et al., 1991). This variant was engineered to add  
82 the following three features to the wild-type SNase: (i) introduction of three stabilizing mutations,  
83 P117G, H124L and S128A (*PHS*); (ii) deletion of amino acids 44-49 and introduction of two  
84 mutations, G50F and V51N ( $\Delta$ ); and (iii) substitution of Val66 with Lys (*V66K*). With these three  
85 modifications, the  $\Delta$ +*PHS/V66K* SNase variant becomes thermally stable, even with the  $\zeta$ -amino  
86 group of Lys-66 entrapped within the hydrophobic cavity originally occupied by the Val-66 side  
87 chain in the wild-type SNase. As a result, the  $\zeta$ -amino group of Lys-66 in the SNase variant exhibits  
88 an unusually low  $\text{pK}_a$  value of 5.7 (García-Moreno et al., 1997; Fitch et al., 2002).

89 Although the SNase variant contains as many as 21 Lys residues (Fig. A1), including the  
90 engineered Lys-66, the  $^{13}\text{C}$ ,  $^1\text{H}$  and  $^{15}\text{N}$  NMR signals for the Lys side chains were unambiguously  
91 observed and assigned by using the SNase variant selectively labeled with SAIL-Lys; i.e., [ $^{13}\text{C}$ ,  
92  $^{15}\text{N}$ ;  $\beta_2, \gamma_2, \delta_2, \epsilon_3$ -D $_4$ ]-Lys (Kainosho et al., 2006; Terauchi et al., 2011). In this article, we  
93 examine some of the structural features inferred from the comprehensive chemical shift data and  
94 the deuterium-induced isotope shifts on the  $^{13}\text{C}^\epsilon$  and  $^{15}\text{N}^\zeta$  of the Lys residues in the SNase variant,  
95 and show that the side chain NMR signals can serve as powerful probes to investigate the *dual*  
96 nature of a Lys side chain in a protein.

## 97 **2 Material and methods**

### 98 **2.1 Sample preparation**

99 The  $\Delta$ +PHS/V66K SNase variants selectively labeled with either [ $^{13}\text{C}$ ,  $^{15}\text{N}$ ]-Lys, [ $^{13}\text{C}$ ,  $^{15}\text{N}$ ;



100  $\beta_2, \gamma_2, \delta_2, \epsilon_3$ -D<sub>4</sub>]-Lys (SAIL-Lys), or [ $\epsilon$ -<sup>13</sup>C; $\epsilon, \epsilon$ -D<sub>2</sub>]-Lys were prepared using the *E. coli* BL21 (DE3)  
101 strain transformed with a pET3 vector (Novagen), encoding the  $\Delta$ +PHS/V66K SNase gene fused  
102 with an N-terminal His-tag. The transformed *E. coli* cells were cultured at 37 °C in 500 mL of M9  
103 medium, containing anhydrous Na<sub>2</sub>HPO<sub>4</sub> (3.4 g/L), anhydrous KH<sub>2</sub>PO<sub>4</sub> (0.5 g/L), NaCl (0.25 g/L),  
104 D-glucose (5 g/L), NH<sub>4</sub>Cl (0.5 g/L), thiamine (0.5 mg/L), FeCl<sub>3</sub> (0.03 mM), MnCl<sub>2</sub> (0.05 mM),  
105 CaCl<sub>2</sub> (0.1 mM), and MgSO<sub>4</sub> (1 mM), with 10 mg/L of the mono-hydrochloride salts of either [U-  
106 <sup>13</sup>C,<sup>15</sup>N]-Lys, SAIL-Lys, or [ $\epsilon$ -<sup>13</sup>C; $\epsilon, \epsilon$ -D<sub>2</sub>]-Lys. Each culture was maintained at 37 °C. An  
107 additional 20 mg/L of each isotope-labeled Lys was supplemented when the OD<sub>600</sub> reached 0.5,  
108 and then protein expression was induced by adding isopropyl- $\beta$ -D-thiogalactopyranoside (IPTG)  
109 to a final concentration of 0.4 mM. At 4-5 h after the induction, the cells were collected by  
110 centrifugation and the SNase variant proteins were purified on a Ni-NTA column according to the  
111 standard protocol. The labeling rates for Lys were ~70%, as measured by mass spectrometry. The  
112 purified proteins were dissolved in 20 mM sodium phosphate buffers containing 100 mM KCl (pH  
113 8.0), prepared with either H<sub>2</sub>O, D<sub>2</sub>O or H<sub>2</sub>O:D<sub>2</sub>O (1:1).

## 114 **2.2 NMR spectroscopy**

115 The 600 MHz 2D <sup>1</sup>H-<sup>13</sup>C constant-time HSQC spectra of the SNase variant, selectively  
116 labeled with either [U-<sup>13</sup>C,<sup>15</sup>N]-Lys or SAIL-Lys, were measured in D<sub>2</sub>O at 30 °C on a Bruker  
117 Avance spectrometer equipped with a TXI cryogenic probe. For the latter sample, additional  
118 deuterium decoupling was applied during the  $t_1$  period. The data sizes and spectral widths were  
119 1,024 ( $t_1$ )  $\times$  2,048 ( $t_2$ ) points and 12,000 Hz ( $\omega_1$ , <sup>13</sup>C)  $\times$  8,700 Hz ( $\omega_2$ , <sup>1</sup>H), respectively. Each set  
120 of 32 scans/FID with a 1.5 s repetition time was collected, using the <sup>13</sup>C carrier frequency at 38  
121 ppm. The 600 MHz 3D HCCH-TOCSY spectrum was measured in D<sub>2</sub>O at 30 °C for the SNase  
122 variant labeled with SAIL-Lys (Clare et al., 1990; Cavanagh et al., 2007). The data size and  
123 spectral width were 1,024 ( $t_1$ )  $\times$  32 ( $t_2$ )  $\times$  2,048 ( $t_3$ ) points and 6,000 Hz ( $\omega_1$ , <sup>1</sup>H) Hz  $\times$  9,100 Hz  
124 ( $\omega_2$ , <sup>13</sup>C)  $\times$  9,000 Hz ( $\omega_3$ , <sup>1</sup>H), respectively. Each set of 16 scans/FID with a 1.5 s repetition time  
125 was collected, using the <sup>13</sup>C carrier frequency at 40 ppm.

126 The Lys  $\zeta$ -<sup>15</sup>N signals of the SAIL-Lys labeled SNase variant dissolved in D<sub>2</sub>O at 30 °C were  
127 assigned using the HECENZ pulse sequence, utilizing the out-and-back magnetization transfer  
128 from <sup>1</sup>H $\epsilon^2$  to <sup>15</sup>N $\zeta$  via <sup>13</sup>C $\epsilon$ . The correlations between the <sup>1</sup>H $\epsilon^2$  and <sup>15</sup>N $\zeta$  signals for most of the 21



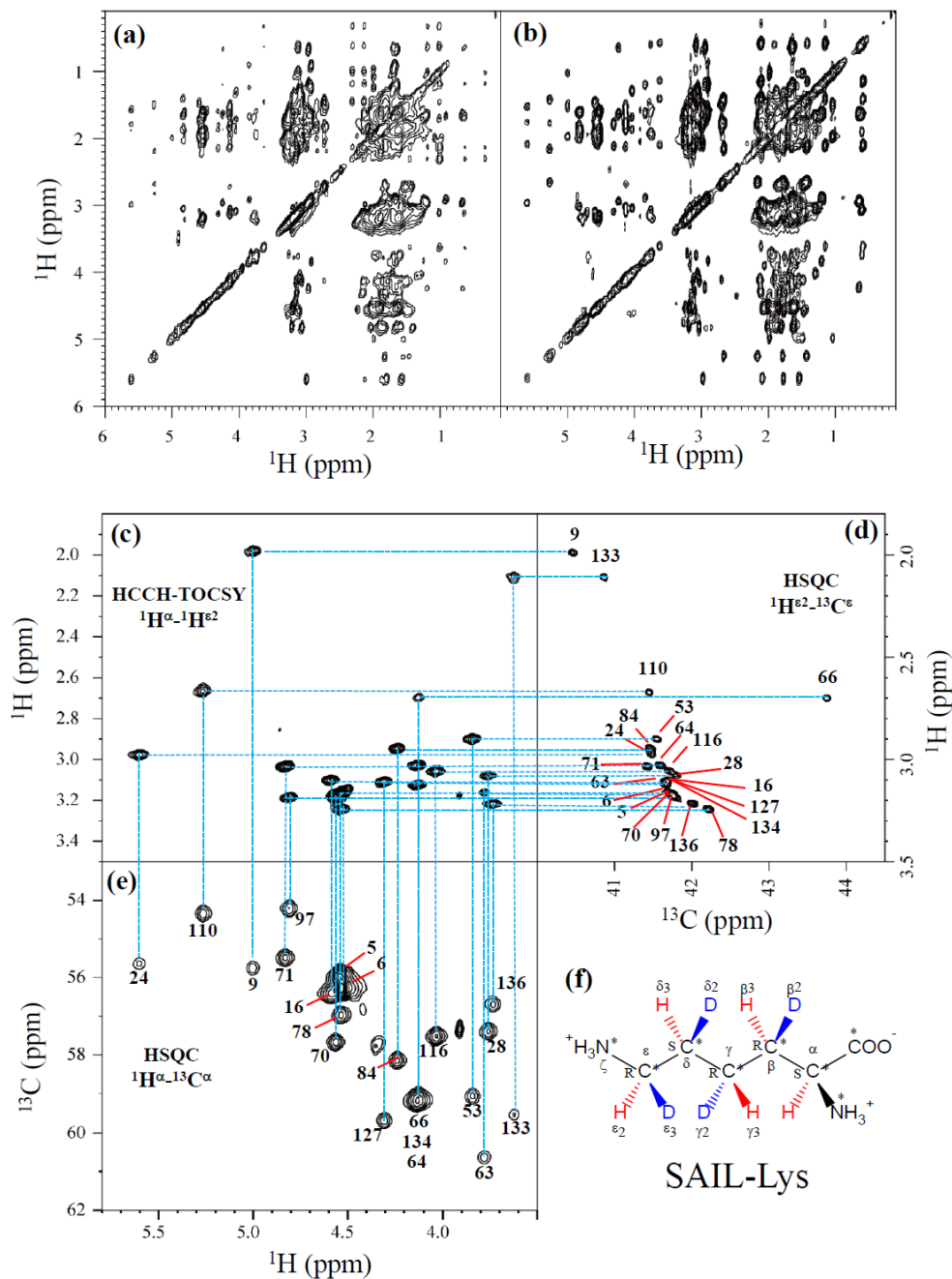
129 Lys residues were firmly established by the pulse sequence, which was basically the same as the  
130 H<sub>2</sub>CN pulse sequence developed by Andre et al. (Andre et al., 2007). The data size and the spectral  
131 width were 512 ( $t_1$ ) × 1024 ( $t_2$ ) points and 1,200 Hz ( $\omega_1$ , <sup>15</sup>N) Hz × 9,600 Hz ( $\omega_2$ , <sup>1</sup>H), respectively,  
132 and deuterium decoupling was applied during the  $t_1$  period. The carrier frequencies were 38 ppm  
133 and 28 ppm for <sup>13</sup>C and <sup>15</sup>N, respectively, and 128 scans/FID with a 2 s repetition time were  
134 accumulated.

135 The 125.7 MHz 1D <sup>13</sup>C NMR spectra of the SNase variant proteins selectively labeled with  
136 either [U-<sup>13</sup>C,<sup>15</sup>N]-Lys or [ $\epsilon$ -<sup>13</sup>C; $\epsilon$ , $\epsilon$ -D<sub>2</sub>]-Lys were measured in D<sub>2</sub>O, H<sub>2</sub>O, and H<sub>2</sub>O-D<sub>2</sub>O (1:1), at  
137 25 °C on a Bruker Avance 500 spectrometer equipped with a DCH cryogenic probe under the  
138 proton and, for the latter sample, simultaneous deuterium decoupling using the WALTZ16 scheme.  
139 The spectral width and repetition time were 6,300 Hz and 5 s, respectively. In the experiment in  
140 H<sub>2</sub>O solution, a 4.1 mm o.d. Shigemi tube containing the protein solution was inserted into a 5 mm  
141 o.d. outer tube containing pure D<sub>2</sub>O for the internal lock signal. By taking advantage of the  
142 selective deuteration on the  $\epsilon$ -<sup>13</sup>C in [ $\epsilon$ -<sup>13</sup>C; $\epsilon$ , $\epsilon$ -D<sub>2</sub>]-Lys (~98 atom %), the background <sup>13</sup>C signals  
143 due to the naturally abundant, and therefore protonated, <sup>13</sup>C nuclei were readily filtered out by  
144 using the pulse scheme shown in Fig. A2.

### 145 **3 Results and discussion**

#### 146 **3.1 Complete assignment of the Lys side chain NMR signals in the SNase variant selectively** 147 **labeled with SAIL-Lys**

148 Although the chemical shifts with sequential assignments for the backbone <sup>1</sup>H, <sup>13</sup>C and <sup>15</sup>N signals  
149 of SNase are available in the BMRB (Entry #16123; Chimenti et al., 2011), we reconfirmed them  
150 by the HNCA experiment for the [U-<sup>13</sup>C, <sup>15</sup>N]-SNase variant, since the solution conditions were  
151 slightly different. The complete side chain assignment for all 21 Lys residues was not trivial, even  
152 for the SNase variant residue-selectively labeled with [U-<sup>13</sup>C, <sup>15</sup>N]-Lys, due to the extensive signal  
153 overlap as illustrated in the *F1-F3* projection of the 3D HCCH TOCSY spectrum (Fig. 1a). On the  
154 other hand, a markedly improved 3D HCCH TOCSY spectrum was obtained, under the  
155 simultaneous deuterium decoupling, for the SNase variant residue-selectively labeled with SAIL-  
156 Lys (Fig. 1b), enabling us to firmly establish the full connectivity for the side chain <sup>1</sup>H, <sup>13</sup>C and



157

158 **Figure 1: Sequential assignment of the Lys side chain signals for the SNase variant selectively**



159 **labeled with SAIL-Lys by the 3D HCCH TOCSY experiment.** Panels (a) and (b) show a  
160 comparison of the *F1-F3* projections of the 3D HCCH TOCSY spectra obtained for the SNase variant  
161 selectively labeled with either [U-<sup>13</sup>C, <sup>15</sup>N]-Lys (a) or SAIL-Lys (b). A complete side chain signal  
162 assignment was established for the SNase variant selectively labeled with SAIL-Lys by the correlation  
163 networks on the 3D HCCH TOCSY spectrum, starting from the backbone <sup>1</sup>H<sup>α</sup>, <sup>13</sup>C<sup>α</sup> signals with  
164 assignments deposited in the BMRB (Entry #16123; Chimenti et al., 2011). For example, the <sup>1</sup>H<sup>ε2</sup>-<sup>13</sup>C<sup>ε</sup>  
165 HSQC signals in panel (d) were unambiguously correlated to the backbone <sup>1</sup>H<sup>α</sup>-<sup>13</sup>C<sup>α</sup> HSQC signals in panel  
166 (e), through the <sup>1</sup>H<sup>α</sup>-<sup>1</sup>H<sup>ε2</sup> correlation signals in panel (c), which represents the *F1-F3* projection of the 3D  
167 HCCH TOCSY spectrum along the <sup>13</sup>C-axis (*F2*) restricted for the <sup>13</sup>C<sup>ε</sup> shift range of 40.1-45.5 ppm. The  
168 structure of SAIL-Lys, [U-<sup>13</sup>C, <sup>15</sup>N; β<sub>2</sub>, γ<sub>2</sub>, δ<sub>2</sub>, ε<sub>3</sub>-D<sub>4</sub>]-Lys, was shown in panel (f). The spectrum was measured  
169 at 30 °C on a Bruker Avance 600 spectrometer equipped with a TXI cryogenic probe.

170 <sup>15</sup>N NMR signals of the 21 Lys residues. To illustrate the improved spectral quality obtained with  
171 the SAIL-Lys in lieu of [U-<sup>13</sup>C, <sup>15</sup>N]-Lys, a panel obtained for the *F1-F3* projection, along the <sup>13</sup>C-  
172 axis (*F2*) restricted for the chemical shift range of 40.1-45.5 ppm for the <sup>13</sup>C<sup>ε</sup> signals, is shown for  
173 the <sup>1</sup>H<sup>α</sup>-<sup>1</sup>H<sup>ε2</sup> correlation signals (Fig. 1c). By taking advantage of the well-dispersed <sup>1</sup>H<sup>α</sup>-<sup>1</sup>H<sup>ε2</sup>  
174 signals, the backbone <sup>1</sup>H<sup>α</sup>-<sup>13</sup>C<sup>α</sup> signals (Fig. 1e) were readily correlated to the <sup>1</sup>H<sup>ε2</sup>-<sup>13</sup>C<sup>ε</sup> HSQC  
175 signals (Fig. 1d). Actually, all of the SAIL-Lys side chain <sup>13</sup>C signals were facilely and  
176 unambiguously assigned through the 3D HCCH TOCSY spectrum, yielding a complete set of the  
177 Lys side chain NMR chemical shifts, as summarized in Table 1. It should be noted that, since each  
178 one of the side chain methylene protons was *stereo-specifically* deuterated in SAIL-Lys; i.e., [U-  
179 <sup>13</sup>C, <sup>15</sup>N; β<sub>2</sub>, γ<sub>2</sub>, δ<sub>2</sub>, ε<sub>3</sub>-D<sub>4</sub>]-Lys (Fig. 1f), all of the 21 Lys side chain methylene proton signals are  
180 *stereo-specifically* assigned to each of the β<sub>3</sub>, γ<sub>3</sub>, δ<sub>3</sub>, and ε<sub>2</sub>-<sup>1</sup>H signals, thus providing precious  
181 clues to examine the local conformations of the Lys side chains in solution.

### 182 **3.2 Structural information inferable from the Lys side chain chemical shifts**

183 Note that the chemical shifts in Table 1 for the 21 Lys residues in the SAIL-Lys labeled SNase  
184 variant are *not* corrected for the various isotope-induced shifts caused by the complicated isotope-  
185 labeling pattern of the SAIL-Lys structure (*see*, Fig. 1f). Based on comprehensive NMR data, we  
186 should be able to elucidate the *dual* role of the Lys side chains in terms of the conformational  
187 dynamics and functional properties of a protein in further detail, using various solution NMR





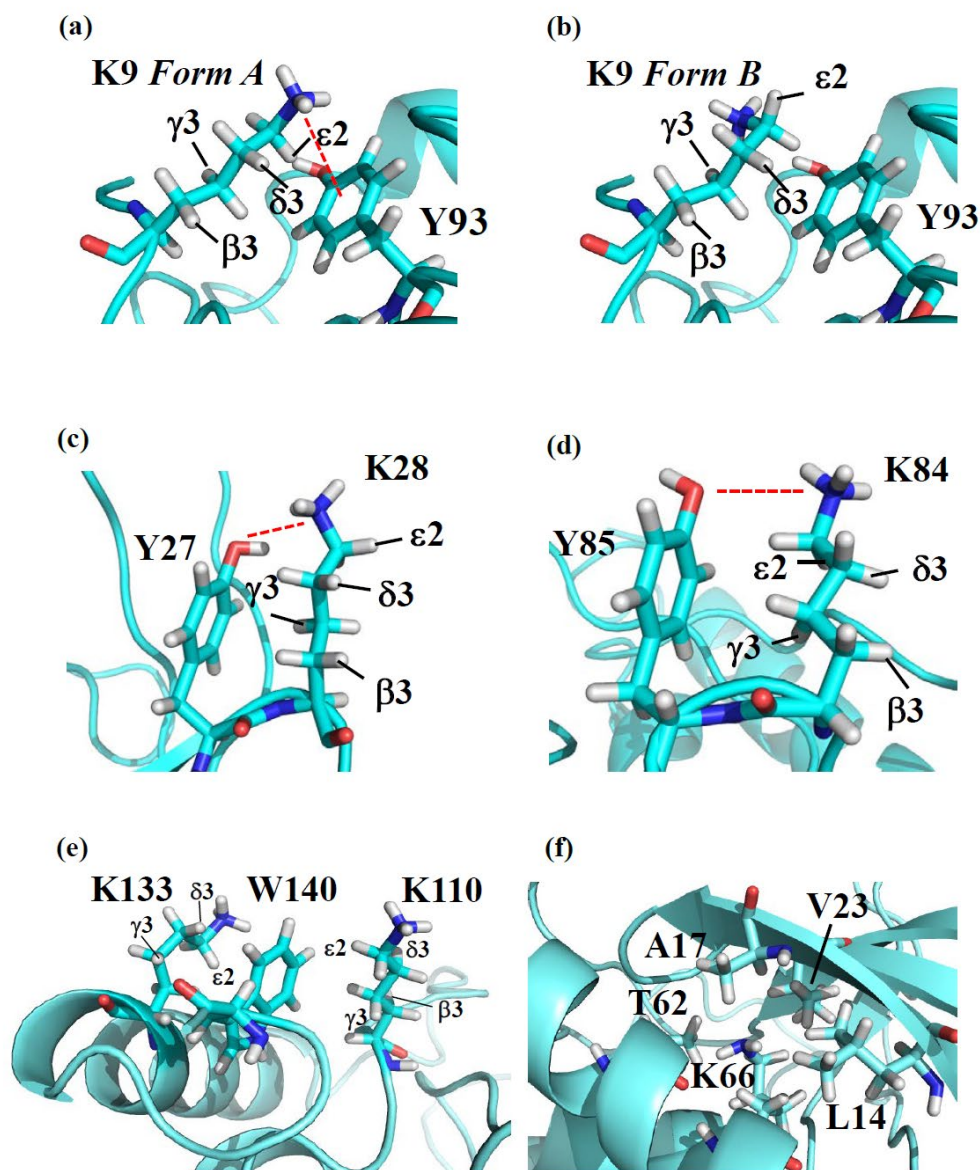
188

|                                         | $^{13}\text{C}^\alpha$ | $^1\text{H}^\alpha$ | $^{13}\text{C}^\beta$ | $^1\text{H}^\beta$ | $^{13}\text{C}^\gamma$ | $^1\text{H}^\gamma$ | $^{13}\text{C}^\delta$ | $^1\text{H}^\delta$ | $^{13}\text{C}^\epsilon$ | $^1\text{H}^\epsilon$ | $^{15}\text{N}^\zeta$ |
|-----------------------------------------|------------------------|---------------------|-----------------------|--------------------|------------------------|---------------------|------------------------|---------------------|--------------------------|-----------------------|-----------------------|
| <b>K5</b>                               | 56.4                   | 4.54                | 32.8                  | 1.98               | 24.1                   | 1.60                | 29.2                   | 1.85                | 41.8                     | 3.17                  | n.d.                  |
| <b>K6</b>                               | 56.0                   | 4.54                | 33.3                  | 1.97               | 24.5                   | 1.63                | 28.4                   | 1.86                | 41.8                     | 3.17                  | n.d.                  |
| <b>K9</b>                               | 55.9                   | 5.00                | 34.5                  | 1.56               | 25.1                   | 1.49                | 28.8                   | 1.04                | 40.5                     | 1.98                  | 30.8                  |
| <b>K16</b>                              | 56.6                   | 4.60                | 35.6                  | 1.92               | 23.9                   | 1.47                | 28.3                   | 1.78                | 41.7                     | 3.10                  | 31.8                  |
| <b>K24</b>                              | 55.8                   | 5.61                | 34.3                  | 2.10               | 25.2                   | 1.54                | 29.5                   | 1.77                | 41.5                     | 2.98                  | 31.8                  |
| <b>K28</b>                              | 57.5                   | 3.80                | 29.5                  | 2.00               | 24.6                   | 0.61                | 29.1                   | 1.63                | 41.9                     | 3.16                  | 32.0                  |
| <b>K53</b>                              | 59.2                   | 3.84                | 31.5                  | 1.64               | 24.7                   | 1.21                | 28.8                   | 1.61                | 41.6                     | 2.90                  | 31.8                  |
| <b>K63</b>                              | 60.8                   | 3.78                | 32.8                  | 1.91               | 24.2                   | 1.46                | 29.7                   | 1.75                | 41.8                     | 3.17                  | n.d.                  |
| <b>K64</b>                              | 59.4                   | 4.13                | 31.8                  | 1.89               | 24.5                   | 1.55                | 28.9                   | 1.74                | 41.6                     | 3.03                  | 31.7                  |
| <b>K66</b>                              | <i>59.5</i>            | <i>4.12</i>         | <i>32.8</i>           | <i>1.85</i>        | <i>25.7</i>            | <i>1.76</i>         | <i>34.0</i>            | <i>1.47</i>         | <i>43.8</i>              | <i>2.70</i>           | <i>20.9</i>           |
| <b>K70</b>                              | 57.8                   | 4.55                | 32.7                  | 1.92               | 24.3                   | 1.60                | 28.6                   | 1.83                | 41.8                     | 3.19                  | n.d.                  |
| <b>K71</b>                              | 55.6                   | 4.84                | 35.2                  | 2.01               | 24.4                   | 1.60                | 28.4                   | 1.82                | 41.4                     | 3.04                  | 31.8                  |
| <b>K78</b>                              | 57.1                   | 4.53                | 33.0                  | 2.06               | 24.1                   | 1.67                | 28.5                   | 1.90                | 42.2                     | 3.24                  | 31.5                  |
| <b>K84</b>                              | 58.3                   | 4.24                | 31.3                  | 1.65               | 23.1                   | 0.64                | 28.8                   | 1.61                | 41.5                     | 2.95                  | 32.0                  |
| <b>K97</b>                              | 54.2                   | 4.81                | 32.9                  | 1.89               | 24.6                   | 1.62                | 28.7                   | 1.79                | 41.8                     | 3.19                  | n.d.                  |
| <b>K110</b>                             | 54.4                   | 5.27                | 35.2                  | 2.17               | 25.1                   | 1.42                | 29.2                   | 1.79                | 41.5                     | 2.68                  | 31.6                  |
| <b>K116</b>                             | 57.7                   | 4.04                | 31.7                  | 1.88               | 24.1                   | 1.30                | 28.5                   | 1.69                | 41.7                     | 3.06                  | 31.7                  |
| <b>K127</b>                             | 59.3                   | 4.31                | 31.9                  | 2.12               | 24.9                   | 1.77                | 29.1                   | 1.83                | 41.7                     | 3.12                  | 31.4                  |
| <b>K133</b>                             | 59.6                   | 3.62                | 32.2                  | 1.42               | 24.1                   | 0.59                | 28.9                   | 1.15                | 40.9                     | 2.10                  | 31.7                  |
| <b>K134</b>                             | 59.4                   | 4.13                | 32.0                  | 2.15               | 24.4                   | 1.65                | 29.5                   | 1.76                | 41.8                     | 3.13                  | 31.6                  |
| <b>K136</b>                             | 56.8                   | 3.76                | 28.8                  | 1.66               | 24.6                   | 1.55                | 28.7                   | 1.95                | 42.0                     | 3.20                  | 31.5                  |
| <b>Avg. <math>\delta</math><br/>ppm</b> | -                      | -                   | <b>33.1</b>           | <b>1.95</b>        | <b>24.5</b>            | <b>1.54</b>         | <b>28.9</b>            | <b>1.68</b>         | <b>41.7</b>              | <b>3.09</b>           | <b>31.7</b>           |

189 **Table 1. The  $^1\text{H}$ ,  $^{13}\text{C}$ ,  $^{15}\text{N}$  chemical shifts for the sidechains of the 21 Lys residues in**  
 190  **$\Delta$ +PHS/V66K SNase selectively labeled with SAIL-Lys in  $\text{D}_2\text{O}$ .** The  $^1\text{H}$  and  $^{13}\text{C}$  signals were assigned  
 191 by the 3D HCCH-TOCSY experiment recorded on a Bruker 600 MHz equipment 30 °C, pH 8.0 using a 600 MHz  
 192 NMR machine. The  $^{15}\text{N}$ -signals were assigned by the HECENZ correlations and those denoted as “n.d.” were not  
 193 clearly observed. Since one of the prochiral methylene protons was stereo-specifically deuterated in the SAIL-Lys, i.e.  
 194  $[\text{U-}^{13}\text{C}, ^{15}\text{N}; \beta_2, \gamma_2, \delta_2, \epsilon_3\text{-D}_4]\text{-Lys}$ , thus the observed  $^1\text{H}$ -signals were unambiguously assigned. The chemical shifts for  
 195 the engineered Lys-66, which has a deprotonated  $\zeta$ -amino group, are shown italic. The averaged chemical shifts are  
 196 obtained by excluding some of the outrageous shifts, and the measurement errors were estimated as less than 0.2 and



197 0.02 ppm, for  $^{13}\text{C}/^{15}\text{N}$ - and  $^1\text{H}$ -chemical shifts, respectively. All chemical shifts are not corrected for the isotope shifts.



198

199 **Figure 2: The local structures around the Lys residues, which exhibit unusual side chain**



200 **chemical shifts, in the crystal structure of the SNase variant (PDB: 3HZX).** The crystal structure  
201 of the SNase variant was solved as a complex with calcium ions and thymidine 3',5'-diphosphate. Therefore,  
202 it may be slightly different from that in the free state. The figures were created with the PyMOL 2.4 software  
203 in order to highlight the relative orientations between the Lys side chains and nearby aromatic rings (a)-(e),  
204 and Lys-66 and the surrounding hydrophobic amino acids (f). The nomenclatures of the prochiral hydrogen  
205 atoms, shown as the suffixes in the figures, are according to the recommended atom identifiers (Markley et  
206 al., 1998).

207 methods. In this section, we briefly interpret the chemical shift data to characterize the local  
208 conformational features by the  $^1\text{H}$ ,  $^{13}\text{C}$ , and  $^{15}\text{N}$ -signals compiled in Table 1, which should be  
209 followed by more extensive studies in the future. Although we have not yet attempted to collect  
210 the comprehensive NOEs, such as by using a *fully* SAIL-labeled SNase variant (Kainosho et al.,  
211 2006), it was obvious that the chemical shift data with exclusive and unambiguous assignments  
212 for the Lys residues contain an abundance of information on the side chain conformations and  
213 ionization states of the  $\zeta$ -amino groups. As described above, the unusual chemical shifts of the  
214 Lys-66 side chain confirmed the deprotonated state of its  $\zeta$ -amino group. We also obtained some  
215 interesting structural information for the other Lys residues with protonated  $\zeta$ -amino groups. For  
216 example, the Lys-9 side chain exists in two conformational states in the crystalline state (PDB  
217 Entry #3HZX), which only differ in the  $\chi^4$ -angle; i.e., *Form A* (*trans*,  $\sim -175^\circ$ ) and *Form B* (*gauche*<sup>+</sup>,  
218  $\sim +44^\circ$ ), as shown in Fig. 2a and b, respectively (*see also*, Table A1). The significantly up-field  
219 shifted signals observed for Lys-9 relative to the averaged chemical shifts ( $\Delta\delta$ , ppm) are obviously  
220 due to the aromatic ring current of Tyr-93; i.e.,  $^{15}\text{N}^\zeta$  (30.8 ppm,  $\Delta\delta = -0.9$  ppm),  $^{13}\text{C}^\epsilon/{}^1\text{H}^{\epsilon 2}$  (40.5/1.98  
221 ppm,  $\Delta\delta = -1.2/-1.11$  ppm) and  ${}^1\text{H}^{\delta 3}$  (1.04 ppm,  $\Delta\delta = -0.64$  ppm). These chemical shifts suggest the  
222  $\zeta\text{-NH}^{3+}\text{-}\pi$  interaction, as shown by the dashed red line (Fig. 2a). Therefore, the chemical shifts for  
223 Lys-9 strongly imply that the *hydrophobic interactions* between the aliphatic side chain, as well as  
224 the *electrostatic interaction* between the positively charged  $\zeta\text{-HN}^{3+}$  and the nearby aromatic ring  
225 of Tyr-93, simultaneously contribute to preferentially stabilize the *Form A* conformation in  
226 solution (Fig. 2a).

227 The high-field shifts of the side chain methylenes, induced by the neighboring aromatic rings,  
228 were also detected for Lys-28, Lys-84 and Lys-133. Considering the local structures of Lys-28 and  
229 Lys-84 in the crystal (Fig. 2c, d), the relative orientations between Lys-28 and Tyr-27, and Lys-84



230 and Tyr-85 seem to be similar to those in the crystal, and are responsible for the large high-field  
231 shifts for only their  $^1\text{H}^{\gamma 3}$  signals; i.e., Lys-28: 0.61 ppm,  $\Delta\delta = -0.93$  ppm; Lys-84: 0.64 ppm,  $\Delta\delta = -$   
232 0.90 ppm, while the other  $^{13}\text{C}/^1\text{H}$  shifts remain within the average ranges (Table 1). The small but  
233 obvious low-field shifts for the  $^{15}\text{N}^{\zeta}$  (Lys-28, Lys-84: 32.0 ppm,  $\Delta\delta = +0.3$  ppm) might be caused  
234 by the electrostatic interactions between the  $\text{O}^{\eta 1}$  of Tyr-27/Tyr-85 and the  $\text{N}^{\zeta}$  of Lys-28/Lys-84,  
235 respectively, as shown by the dashed red lines (Fig. 2 c, d). The bulky indole ring of Trp-140 seems  
236 to simultaneously stabilize the aliphatic chains of both Lys-133 and Lys-110, inducing the high-  
237 field shifts for some of the side chain signals; i.e., Lys-133  $^{13}\text{C}^{\varepsilon}/^1\text{H}^{\varepsilon 2}$  (40.9/2.10 ppm,  $\Delta\delta = -0.8/-$   
238 0.99 ppm),  $^1\text{H}^{\delta 3}$  (1.15 ppm,  $\Delta\delta = -0.53$  ppm),  $^1\text{H}^{\gamma 3}$  (0.59 ppm,  $\Delta\delta = -0.95$  ppm) and  $^1\text{H}^{\beta 3}$  (1.42 ppm,  
239  $\Delta\delta = -0.53$  ppm); Lys-110  $^1\text{H}^{\varepsilon 2}$  (2.68 ppm,  $\Delta\delta = -0.41$  ppm). These up-field shifted signals indicate  
240 that the hydrophobic interactions between the methylene moieties of Lys-133 and Lys-110, with  
241 the hydrophobic indole ring of Trp-140 sandwiched in the middle, are also preserved in solution  
242 (Fig. 2e). Interestingly, the chemical shift differences between the two prochiral methylene protons  
243 attached to the  $\varepsilon$ -carbons of the Lys residues, observed for the SNase variant residue-selectively  
244 labeled with  $[\text{U-}^{13}\text{C}, ^{15}\text{N}]$ -Lys, are only considerably large for the Lys-110 and -133 residues, while  
245 those for the other 19 Lys residues were much smaller than  $\sim 0.05$  ppm, if present (Fig. A3). Since  
246 the  $^1\text{H}^{\varepsilon 2}$  chemical shifts were observed at 0.15 and 0.17 ppm higher field than the  $^1\text{H}^{\varepsilon 3}$  chemical  
247 shifts for Lys-110 and -133, respectively, the conformations of these two Lys residues are likely to  
248 be similar to those in the crystal (Fig. 2e).

249 On the other hand, the striking chemical shifts observed for the Lys-66 residue, which is  
250 deliberately trapped within the hydrophobic environment engineered in the SNase variant (Fig. 2f),  
251 clearly reveal the strong influence of the ionization state of the  $\zeta$ -amino group on the Lys side  
252 chain chemical shifts. As shown in Table 1, the  $^{15}\text{N}^{\zeta}$  chemical shift of the  $\zeta$ - $\text{ND}_2$  of Lys-66 in the  
253 SNase variant appears at an unusually high-field position, as compared to the averaged chemical  
254 shift range for the  $\zeta$ - $\text{ND}^{3+}$  in the other Lys residues; i.e.,  $^{15}\text{N}^{\zeta}$  (Lys-66: 20.9 ppm,  $\Delta\delta = -10.8$  ppm),  
255 which is close to the value of the  $\zeta$ - $\text{NH}_2$  chemical shift, 23.3 ppm, previously reported for Lys-66  
256 in the  $[\text{U-}^{13}\text{C}, ^{15}\text{N}]$ -SNase variant (André et al., 2007; Takayama et al., 2008). Apparently, the  $^{15}\text{N}^{\zeta}$   
257 chemical shifts provide a quite useful clue to distinguish between the deprotonated and protonated  
258  $\zeta$ -amino groups of Lys residues, given that the complete side chain assignment including the



259 terminal  $\zeta$ - $^{15}\text{N}$  signals by conventional methods using a  $[\text{U-}^{13}\text{C},^{15}\text{N}]$ -protein is usually laborious,  
260 and occasionally impossible.

261 The deprotonation of the  $\zeta$ -amino group caused sizable  $^1\text{H}$  and  $^{13}\text{C}$  chemical shift changes  
262 down to the  $\gamma$ -position in the side chain, as observed for Lys-66; i.e.,  $^{13}\text{C}^\epsilon/{}^1\text{H}^{\epsilon 2}$  (43.8/2.70 ppm,  
263  $\Delta\delta = +2.1/-0.39$  ppm),  $^{13}\text{C}^\delta/{}^1\text{H}^{\delta 3}$  (34.0/1.47 ppm,  $\Delta\delta = +5.1/-0.21$  ppm), and  $^{13}\text{C}^\gamma/{}^1\text{H}^{\gamma 3}$  (25.7/1.76  
264 ppm,  $\Delta\delta = +1.2/+0.22$  ppm). These *deprotonation* shifts, especially on the  $^{13}\text{C}^\epsilon$  and/or  $^{13}\text{C}^\delta$   
265 chemical shifts, could therefore be used as a useful alternative index to characterize the ionization  
266 states of the  $\zeta$ -amino groups of Lys residues in a protein, since they can be accurately and readily  
267 observed and assigned by using a protein selectively labeled with SAIL-Lys. It should be noted,  
268 however, that the side chain chemical shifts in general might significantly vary according to the  
269 local environments, such as the relative position to aromatic rings, and thus the results obtained  
270 exclusively from the side chain chemical shifts might not be absolutely reliable. To avoid any  
271 possible uncertainties in characterizing the ionization states of  $\zeta$ -amino groups, an alternative  
272 approach using the deuterium-induced isotope shifts of the SAIL-Lys side chain  $^{13}\text{C}$  signals must  
273 be developed.

### 274 **3.3 Characterization of the ionization state of the $\zeta$ -amino group of Lys residues using the** 275 **effects of deuterium-induced isotope shifts on the side chain $^{13}\text{C}$ and $^{15}\text{N}$ signals**

276 In our previous studies investigating the effects of the deuterium-induced isotope shifts on  
277 the  $^{13}\text{C}$  signals adjacent to polar functional groups with an exchangeable hydrogen, such as  
278 hydroxyl (OH) or sulfhydryl (SH) groups, we demonstrated that those isotope shifts are versatile  
279 indices for identifying residues, such as Tyr, Thr, Ser or Cys, with *exceptionally* slow hydrogen  
280 exchange rates (Takeda et al., 2014). For example, in a protein selectively labeled with  $[\zeta\text{-}^{13}\text{C}]$ -  
281 Tyr, the Tyr residues have much slower hydrogen exchange rates for the  $\eta$ -hydroxyl groups than  
282 the isotope shift differences in the  $^{13}\text{C}^\zeta$  signals, and exhibit well-resolved pairwise signals with  
283 nearly equal intensities in the 1D  $^{13}\text{C}$ -NMR spectrum in  $\text{H}_2\text{O}$ - $\text{D}_2\text{O}$  (1:1) (Takeda et al., 2009). The  
284 up- and downfield counterparts of the pairwise  $^{13}\text{C}^\zeta$  signals correspond to those in  $\text{D}_2\text{O}$  and  $\text{H}_2\text{O}$ ,  
285 respectively, and their relative intensities reflect the fractionation factors; i.e.,  $[\text{OD}]/[\text{OH}]$ . Similar  
286 approaches have been developed for Ser, Thr and Cys residues, using the  $^{13}\text{C}^\beta$  signals observed for

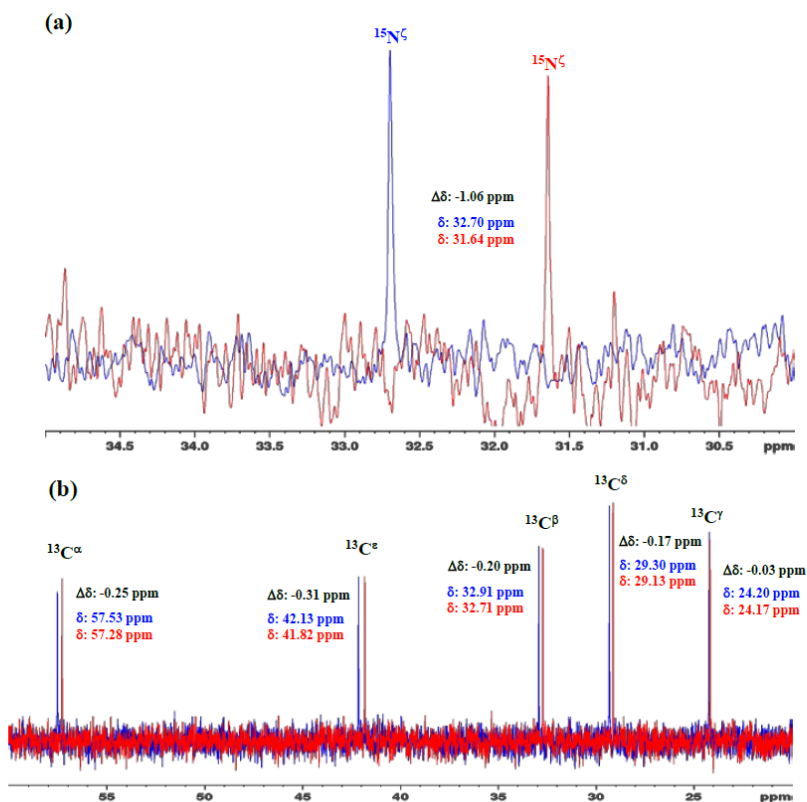


287 proteins selectively labeled with [ $\beta$ - $^{13}\text{C}$ ;  $\beta$ ,  $\beta$ -D $_2$ ]-Ser, [ $\beta$ - $^{13}\text{C}$ ;  $\beta$ -D]-Thr, and [ $\beta$ - $^{13}\text{C}$ ;  $\beta$ ,  $\beta$ -D $_2$ ]-Cys,  
288 respectively (Takeda et al., 2010, 2011). Since the isolated  $^{13}\text{C}^\beta(\text{D}_2)$  or  $^{13}\text{C}^\beta(\text{D})$  moieties in the  
289 labeled amino acids give extremely narrow signals under the deuterium decoupling, the  $^{13}\text{C}$ -NMR  
290 signals can be obtained with remarkably high sensitivities, especially with a  $^{13}\text{C}$ -direct observing  
291 cryogenic probe. Interestingly, while the fractionation factors for the Ser and Thr hydroxyl groups;  
292 i.e., [OD]/[OH], are usually close to unity, as also for the Tyr residues, those for the Cys sulfhydryl  
293 groups; i.e., [SD]/[SH], are around 0.4-0.5 (Takeda et al., 2010, 2011). The methods are especially  
294 important, since the functional groups of the residues readily identified as having exceptionally  
295 slow hydrogen exchange rates are most likely to be involved in hydrogen bonding networks and/or  
296 located in distinctive local environments.

297 Although the idea of estimating the hydrogen exchange rates by the deuterium-induced  
298 isotope shifts on the  $^{13}\text{C}$  nuclei adjacent to functional groups with exchangeable hydrogens was  
299 originally exploited years ago, for the backbone amide groups in the residue-selectively labeled  
300 proteins with [ $\text{C}'$ - $^{13}\text{C}$ ]-amino acid(s) (Kainosho and Tsuji 1982; Markley and Kainosho, 1993), it  
301 has not yet been applied for the Lys  $\zeta$ -amino groups. Having established the complete assignment  
302 for the 21 Lys residues in the SNase variant selectively labeled with SAIL-Lys (Table 1), we next  
303 examined the deuterium-induced chemical shifts in detail for the Lys side chain signals. In the case  
304 of Lys residues, the NMR signals of the  $\zeta$ -amino  $^{15}\text{N}$  and  $\epsilon$ - or  $\delta$ -carbon  $^{13}\text{C}$  signals would be  
305 plausible candidates for probing the deuterium substitution effects. There have only been a few  
306 reports on the isotope shifts of the  $\delta$ - and  $\epsilon$ - $^{13}\text{C}$  for the Lys-residues induced by the deuteration of  
307  $\zeta$ -amino groups (Hansen, 1983; Dziembowska et al., 2004). However, apparently no  
308 comprehensive studies have applied the deuterium-induced isotope shifts to characterize the  
309 ionization states of Lys residues.

310 We first examined the 1D  $^{13}\text{C}$ - and  $^{15}\text{N}$ -NMR spectra of [ $^{15}\text{N}_2$ ]-Lys in D $_2\text{O}$  and H $_2\text{O}$ , at pH 8 and  
311 30 °C, to choose the suitable NMR probes to distinguish between the deprotonated and  
312 protonated  $\zeta$ -amino groups (Fig. 3). The  $\zeta$ - $^{15}\text{N}$  signal appears at  $\sim 1$  ppm up-field in D $_2\text{O}$  relative  
313 to that in H $_2\text{O}$  (Fig. 3a), and the aliphatic  $^{13}\text{C}$  signals of [ $^{15}\text{N}_2$ ]-Lys at the natural abundance also  
314 showed isotope shifts,  $\Delta\delta[^{13}\text{C}^i(\text{in D}_2\text{O}) - \delta^{13}\text{C}^i(\text{in H}_2\text{O})]$ ; i.e.,  $^{13}\text{C}^\alpha$ , -0.25 ppm;  $^{13}\text{C}^\beta$ , -0.20 ppm;  
315  $^{13}\text{C}^\gamma$ , -0.03 ppm;  $^{13}\text{C}^\delta$ , -0.17 ppm; and  $^{13}\text{C}^\epsilon$ , -0.31 ppm (Fig. 3b). Although the isotope shifts for





316

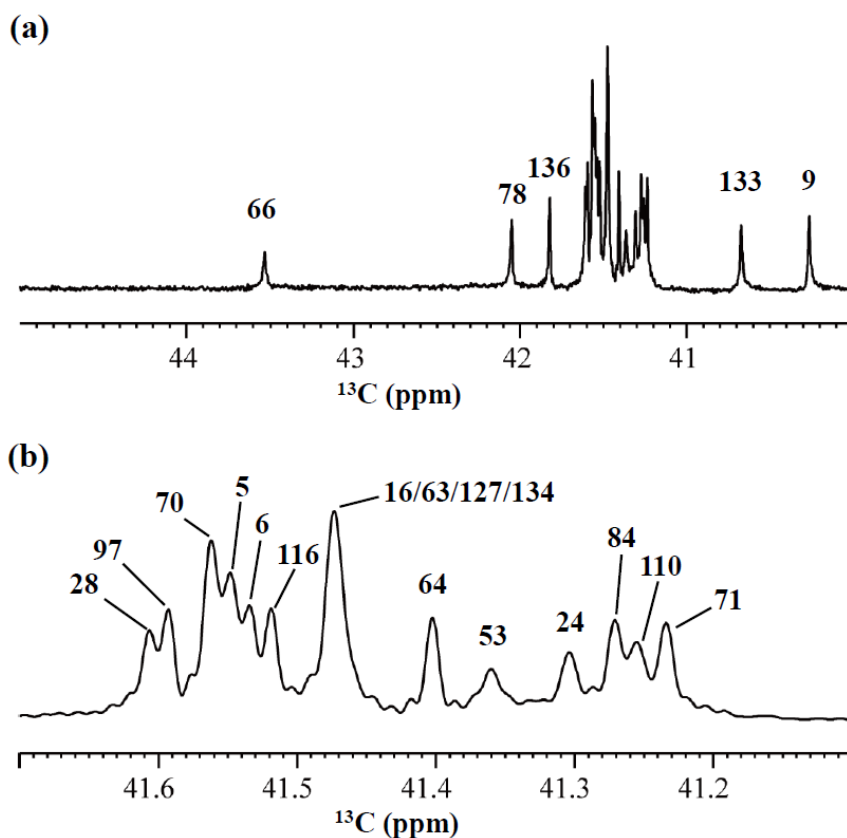
317 **Figure 3: 1D  $^{15}\text{N}$ - and  $^{13}\text{C}$ -NMR spectra of  $^{15}\text{N}_2$ -lysine free in  $\text{H}_2\text{O}$  and  $\text{D}_2\text{O}$ .** The 96.3 MHz  
318 1D  $^{15}\text{N}$ -NMR spectra (Figure 3a) and 239.0 MHz 1D  $^{13}\text{C}$ -NMR spectra (Figure 3b) of  $^{15}\text{N}_2$ -lysine were  
319 measured at 30 °C on a Bruker Avance III 950 spectrometer with a TCI cryogenic probe, using ~70 mM  
320 solutions of either 20 mM Tris buffer prepared with  $\text{H}_2\text{O}$  (or  $\text{D}_2\text{O}$ ) at pH (or pD) 8.0. The NMR spectra and  
321 the chemical shifts,  $\delta$  ppm, shown in blue and red, are those for the  $\text{H}_2\text{O}$  and  $\text{D}_2\text{O}$  buffer solutions,  
322 respectively. The deuterium-induced shifts,  $\Delta\delta$  ppm :  $\delta$  (in  $\text{D}_2\text{O}$ ) -  $\delta$  (in  $\text{H}_2\text{O}$ ) for the  $^{15}\text{N}_\zeta$  and side chain  $^{13}\text{C}$   
323 signals are shown in black.

324  $^{13}\text{C}^\alpha$  and  $^{13}\text{C}^\beta$  are due to the deuteration of the  $\alpha$ -amino group, those for  $^{13}\text{C}^\delta$  and  $^{13}\text{C}^\epsilon$  are obviously  
325 due to the deuteration of the  $\zeta$ -amino group. Considering the finding that the  $^{13}\text{C}^\epsilon$  of Lys gives an  
326 isolated signal far from the others and exhibits a ~1.8-fold larger isotope shift as compared to  $^{13}\text{C}^\delta$ ,



327 the  $^{13}\text{C}^\epsilon$  and  $^{15}\text{N}^\zeta$  signals seem to be good candidates for probing the ionization states of Lys  
328 residues in the SNase variant.

329 Although the  $^{15}\text{N}^\zeta$  and  $^{13}\text{C}^\epsilon$  chemical shifts for the Lys residues can be measured by the HECENZ  
330 and  $^1\text{H}$ - $^{13}\text{C}$  ct-HSQC experiments, respectively, using the SNase variant selectively



331  
332 **Figure 4: 125.7 MHz  $\{^1\text{H}, ^2\text{D}\}$ -decoupled 1D- $^{13}\text{C}$ -NMR spectrum for the SNase variant**  
333 **selectively labeled with  $[\epsilon\text{-}^{13}\text{C}; \epsilon,\epsilon\text{-D}_2]$ -Lys.** The spectra were measured at 25 °C, pH 8.0, in  $\text{D}_2\text{O}$   
334 solution on an Avance 500 spectrometer equipped with a DCH cryogenic probe. Although only a  
335 few discrete  $^{13}\text{C}^\epsilon$  signals are apparent in Figure 4a, the congested spectral region around 41-42 ppm  
336 shows well-separated signals due to their narrow line-widths of 1-2 Hz (Figure 4b). All of the 1D  
337 NMR signals for  $^{13}\text{C}^\epsilon$  were readily assigned by using the chemical shift data obtained from the 3D  
338 HCCH TOCSY experiment for the SNase variant selectively labeled with SAIL-Lys (*see* Sect. 3.1).





339 labeled with [U-<sup>13</sup>C, <sup>15</sup>N]-Lys or SAIL-Lys, it was rather difficult to determine the accurate isotope  
 340 shifts of the <sup>15</sup>N<sup>ζ</sup> and <sup>13</sup>C<sup>ε</sup> signals for all 21 Lys residues by these methods. Especially, the accurate  
 341 chemical shift measurement for an individual <sup>13</sup>C<sup>ε</sup> signal was hampered by the insufficient quality

|                                       | $\delta^{15}\text{N}^{\zeta}$<br>in H <sub>2</sub> O | $\delta^{15}\text{N}^{\zeta}$<br>in D <sub>2</sub> O | $\Delta\delta^{15}\text{N}^{\zeta}$<br>ppm | $\delta^{13}\text{C}^{\epsilon}$<br>in H <sub>2</sub> O | $\delta^{13}\text{C}^{\epsilon}$<br>in D <sub>2</sub> O | $\Delta\delta^{13}\text{C}^{\epsilon}$<br>ppm |
|---------------------------------------|------------------------------------------------------|------------------------------------------------------|--------------------------------------------|---------------------------------------------------------|---------------------------------------------------------|-----------------------------------------------|
| <b>K5</b>                             | n.d.                                                 | n.d.                                                 | n.d.                                       | 41.89                                                   | 41.54                                                   | -0.35                                         |
| <b>K6</b>                             | n.d.                                                 | n.d.                                                 | n.d.                                       | 41.87                                                   | 41.53                                                   | -0.34                                         |
| <b>K9</b>                             | 31.9                                                 | 30.8                                                 | -1.1                                       | 40.55                                                   | 40.26                                                   | -0.29                                         |
| <b>K16</b>                            | 32.9                                                 | 31.8                                                 | -1.1                                       | 41.80                                                   | 41.47                                                   | -0.33                                         |
| <b>K24</b>                            | 33.1                                                 | 31.8                                                 | -1.3                                       | 41.66                                                   | 41.31                                                   | -0.35                                         |
| <b>K28</b>                            | 33.0                                                 | 32.0                                                 | -1.0                                       | 41.92                                                   | 41.62                                                   | -0.30                                         |
| <b>K53</b>                            | 32.9                                                 | 31.8                                                 | -1.1                                       | n.d.                                                    | 41.36                                                   | n.d.                                          |
| <b>K63</b>                            | n.d.                                                 | n.d.                                                 | n.d.                                       | 41.80                                                   | 41.47                                                   | -0.33                                         |
| <b>K64</b>                            | 32.7                                                 | 31.7                                                 | -1.0                                       | 41.72                                                   | 41.41                                                   | -0.31                                         |
| <b>K66</b>                            | 22.7                                                 | 20.9                                                 | -1.8                                       | 43.75                                                   | 43.54                                                   | -0.21                                         |
| <b>K70</b>                            | n.d.                                                 | n.d.                                                 | n.d.                                       | 41.89                                                   | 41.55                                                   | -0.34                                         |
| <b>K71</b>                            | 32.8                                                 | 31.8                                                 | -1.0                                       | 41.55                                                   | 41.24                                                   | -0.31                                         |
| <b>K78</b>                            | 32.7                                                 | 31.5                                                 | -1.2                                       | 42.37                                                   | 42.09                                                   | -0.28                                         |
| <b>K84</b>                            | 33.1                                                 | 32.0                                                 | -1.1                                       | 41.64                                                   | 41.36                                                   | -0.28                                         |
| <b>K97</b>                            | n.d.                                                 | n.d.                                                 | n.d.                                       | 41.91                                                   | 41.59                                                   | -0.32                                         |
| <b>K110</b>                           | 32.8                                                 | 31.6                                                 | -1.2                                       | 41.65                                                   | 41.26                                                   | -0.39                                         |
| <b>K116</b>                           | 32.8                                                 | 31.7                                                 | -1.1                                       | 41.86                                                   | 41.52                                                   | -0.34                                         |
| <b>K127</b>                           | 32.6                                                 | 31.4                                                 | -1.2                                       | 41.80                                                   | 41.50                                                   | -0.30                                         |
| <b>K133</b>                           | 32.8                                                 | 31.7                                                 | -1.1                                       | 40.96                                                   | 40.67                                                   | -0.29                                         |
| <b>K134</b>                           | 32.6                                                 | 31.6                                                 | -1.0                                       | 41.80                                                   | 41.50                                                   | -0.30                                         |
| <b>K136</b>                           | 32.5                                                 | 31.5                                                 | -1.0                                       | 42.12                                                   | 41.82                                                   | -0.30                                         |
| Avg. $\delta$ ,<br>$\Delta\delta$ ppm | 32.7                                                 | 31.6                                                 | -1.1<br>+/- 0.1                            | 41.72                                                   | 41.40                                                   | -0.32<br>+/- 0.02                             |

342 **Table 2. Deuterium-induced isotope shifts for the sidechain <sup>15</sup>N<sup>ζ</sup> and <sup>13</sup>C<sup>ε</sup> signals of the 21**  
 343 **Lys residues in Δ+PHS/V66K SNase.** The <sup>15</sup>N<sup>ζ</sup> and <sup>13</sup>C<sup>ε</sup> chemical shift data in H<sub>2</sub>O and D<sub>2</sub>O were obtained  
 344 for the SNase labeled either with SAIL-Lys or [ε-<sup>13</sup>C; ε,ε-D<sub>2</sub>]-Lys, respectively. Note that the 1D <sup>13</sup>C<sup>ε</sup> data measured  
 345 at 125.7 MHz the 1D <sup>13</sup>C-spectra are much higher precision as compared to those by the 2D HSQC using the SNase  
 346 labeled with SAIL-Lys. The averaged chemical shifts in the last row are obtained for the Lys residues with protonated

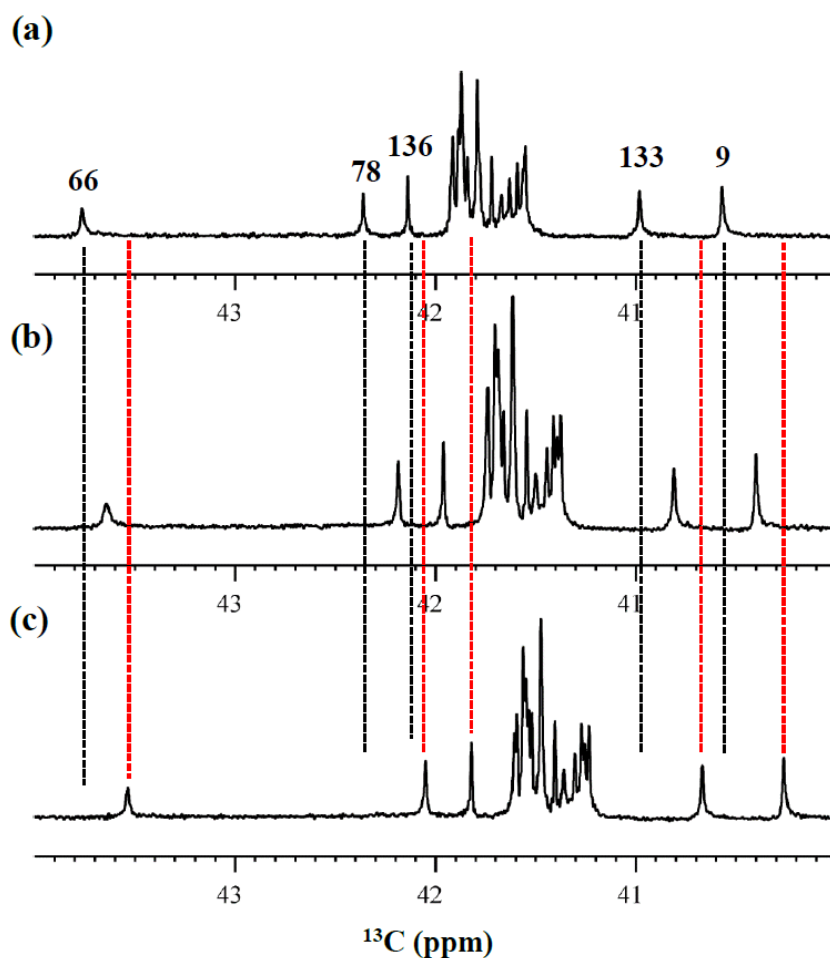


347  $\zeta$ -amino groups, except for Lys-66 (*italic*) which has a deprotonated  $\zeta$ -amino group. The averaged  $\Delta\delta$  values show the  
348 difference between the averaged  $^{15}\text{N}^\zeta$  and  $^{13}\text{C}^\epsilon$ , except for Lys-66 which are the difference between its  $^{15}\text{N}^\zeta$  and  $^{13}\text{C}^\epsilon$   
349 shifts in  $\text{H}_2\text{O}$  and  $\text{D}_2\text{O}$ . Negative  $\Delta\delta$  values indicate the chemical shifts in  $\text{D}_2\text{O}$  are up-field shifted due to deuteration  
350 of the  $\zeta$ -amino groups.

351 of the ct-HSQC spectrum, even for the protein labeled with SAIL-Lys (Fig. A3). Therefore, we  
352 used  $[\epsilon\text{-}^{13}\text{C}; \epsilon, \epsilon\text{-D}_2]\text{-Lys}$  to reduce the line-widths of the  $^{13}\text{C}^\epsilon$  signals for the Lys-residues in the  
353 SNase variant. As expected, the 1D  $^{13}\text{C}$ -NMR spectra of the SNase variant selectively labeled with  
354  $[\epsilon\text{-}^{13}\text{C}; \epsilon, \epsilon\text{-D}_2]\text{-Lys}$  showed remarkably well-resolved signals with line-widths less than 2 Hz,  
355 under the  $^1\text{H}/^2\text{D}$  double decoupling conditions (Fig. 4). Note that the weak background signals due  
356 to the naturally abundant  $^{13}\text{C}$  nuclei were filtered out in this spectrum (Fig. A2). By referring to  
357 the chemical shifts in Table 1, which were determined by the 3D HCCH TOCSY experiment for  
358 the SNase labeled with SAIL-Lys, all of the 1-D  $^{13}\text{C}^\epsilon$  signals were unambiguously assigned (Fig.  
359 4 a, b). The chemical shifts of  $^{13}\text{C}^\epsilon$  are slightly different among the data sets, because the isotope  
360 shifts induced by the nearby isotopes on the  $^{13}\text{C}^\epsilon$  signals are different for SAIL-Lys and  $[\epsilon\text{-}^{13}\text{C}; \epsilon,$   
361  $\epsilon\text{-D}_2]\text{-Lys}$  (Tables 1, 2). The  $^{13}\text{C}^\epsilon$  chemical shifts in  $\text{H}_2\text{O}$  and  $\text{D}_2\text{O}$ , which were accurately  
362 determined by the 1D  $^{13}\text{C}$ -NMR spectra, are presented in Fig. 5. At a glance, the  $^{13}\text{C}^\epsilon$  spectra in  
363 Fig. 5a and 5c look almost the same, since the signals moved up-field with a constant increment  
364 of  $-0.32 \pm 0.02$  ppm, except for the  $^{13}\text{C}^\epsilon$  signal of Lys-66 (Table 2). Since the  $\delta^{13}\text{C}^\epsilon$  values in  $\text{H}_2\text{O}$   
365 and  $\text{D}_2\text{O}$  are very close to those for the *free*  $[\text{N}_2]\text{-Lys}$  (Fig. 3b), the  $\zeta$ -amino groups are protonated  
366 in  $\text{H}_2\text{O}$  and deuterated in  $\text{D}_2\text{O}$ , and thus the averaged deuterium-induced isotope shift was  
367 designated as  $\Delta\delta^{13}\text{C}^\epsilon [\text{N}^\zeta\text{D}_3^+ \text{-N}^\zeta\text{H}_3^+]$ . Similarly, the averaged  $\Delta\delta^{15}\text{N}^\zeta [\text{N}^\zeta\text{D}_3^+ \text{-N}^\zeta\text{H}_3^+]$ , excluding the  
368 value for Lys-66, was determined to be  $-1.1 \pm 0.1$  ppm, which was also close to the *free*  $[\text{N}_2]\text{-}$   
369 Lys (Fig. 3a). The  $\Delta\delta^{13}\text{C}^\epsilon$  and  $\Delta\delta^{15}\text{N}^\zeta$  for Lys-66, which are  $-0.21$  and  $-1.8$  ppm (Table 2),  
370 respectively, confirmed that the  $\zeta$ -amino group of this residue is deprotonated at pH 8, and should  
371 be designated as  $\Delta\delta^{13}\text{C}^\epsilon [\text{N}^\zeta\text{D}_2 \text{-N}^\zeta\text{H}_2]$  and  $\Delta\delta^{15}\text{N}^\zeta [\text{N}^\zeta\text{D}_2 \text{-N}^\zeta\text{H}_2]$ . Interestingly, the fact that the  
372 averaged  $\Delta\delta^{13}\text{C}^\epsilon [\text{N}^\zeta\text{D}_3^+ \text{-N}^\zeta\text{H}_3^+]$ ,  $-0.32$  ppm, was  $\sim 1.5$  times larger than the  $\Delta\delta^{13}\text{C}^\epsilon [\text{N}^\zeta\text{D}_2 \text{-N}^\zeta\text{H}_2]$   
373 for Lys-66,  $-0.21$  ppm, might suggest that the deuterium-induced isotope shift on  $^{13}\text{C}^\epsilon$  is  
374 proportional to the number of hydrogen atoms on the  $\zeta$ -amino groups. In contrast, the averaged  
375  $\Delta\delta^{15}\text{N}^\zeta [\text{N}^\zeta\text{D}_3^+ \text{-N}^\zeta\text{H}_3^+]$ ,  $-1.1$  ppm, was much smaller than that of the  $\Delta\delta^{15}\text{N}^\zeta [\text{N}^\zeta\text{D}_2 \text{-N}^\zeta\text{H}_2]$  for Lys-66, -  
376 1.8 ppm.



377 We also measured the 1D  $^{13}\text{C}$ -NMR spectrum of the SNase variant selectively labeled with  $[\epsilon\text{-}^{13}\text{C};$   
378  $\epsilon, \epsilon\text{-D}_2]$ -Lys in  $\text{H}_2\text{O}\text{-D}_2\text{O}$  (1:1), to search for the Lys residues with slowly exchanging  $\zeta$ -amino  
379 groups. Obviously, there are no such residues in the SNase variant at pH 8 and 30 °C, as



380  
381 **Figure 5: Isotope shifts on the  $^{13}\text{C}^\epsilon$  signals of the Lys residues in the SNase variant selectively**  
382 **labeled with  $[\epsilon\text{-}^{13}\text{C};\epsilon,\epsilon\text{-D}_2]$ -Lys, caused by the deuterium substitutions for the  $\zeta$ -amino**  
383 **groups.** The 125.7 MHz  $\{^1\text{H}, ^2\text{D}\}$ -decoupled 1D  $^{13}\text{C}$  NMR spectra were measured at 25 °C, pH  
384 8.0, in either  $\text{H}_2\text{O}$  (Figure 5a),  $\text{H}_2\text{O}:\text{D}_2\text{O}$  (1:1) (Figure 5b), or  $\text{D}_2\text{O}$  (Figure 5c) solutions on an  
385 Avance 500 spectrometer equipped with a DCH cryogenic probe in  $\text{H}_2\text{O}$  (a),  $\text{H}_2\text{O}:\text{D}_2\text{O}$  (1:1) (b),



386 and D<sub>2</sub>O (c) solutions. The vertical black and red dotted lines show the chemical shifts observed  
387 in 100% H<sub>2</sub>O and D<sub>2</sub>O, respectively. The complete data for the deuterium-induced isotope shifts  
388 for the sidechain <sup>15</sup>N<sup>ε</sup> and <sup>13</sup>C<sup>ε</sup> signals are summarized in Table 2.

389 shown in Fig. 5b. Due to the rapid hydrogen exchange rates for all 21 Lys residues in this  
390 protein, the observed isotope shifts on <sup>13</sup>C<sup>ε</sup> were exactly half of the  $\Delta\delta^{13}\text{C}^\epsilon$  [<sup>N<sup>ε</sup>D<sub>2</sub>-N<sup>ε</sup>H<sub>2</sub></sup>] for Lys-  
391 66 or  $\Delta\delta^{13}\text{C}^\epsilon$  [<sup>N<sup>ε</sup>D<sub>3</sub><sup>+</sup>-N<sup>ε</sup>H<sub>3</sub><sup>+</sup></sup>] for the rest of the Lys residues. The hydrogen exchange rate (*K<sub>ex</sub>*) for  
392 the ζ-amino group of Lys-66 in the SNase variant, which is deeply embedded in the hydrophobic  
393 cavity originally occupied by Val-66 in the wild-type SNase, was 93+/-5 S<sup>-1</sup> at pH 8 and -1 °C  
394 (Takayama et al., 2008). Therefore, the hydrogens on the ζ-amino groups in all 21 Lys residues in  
395 the SNase variant are rapidly exchanging, and thus the observed chemical shifts for the <sup>13</sup>C<sup>ε</sup> of  
396 Lys-66 and the rest of the Lys residues in H<sub>2</sub>O-D<sub>2</sub>O (1:1 ) are the time-averages for three  
397 isotopomers, NH<sub>2</sub>, NHD, and ND<sub>2</sub>, with nearly a 1:2:1 ratio for Lys-66, and for four isotopomers,  
398 NH<sub>3</sub><sup>+</sup>, NH<sub>2</sub>D<sup>+</sup>, NHD<sub>2</sub><sup>+</sup>, and ND<sub>3</sub><sup>+</sup>, with a ratio of 1:3:3:1. Since the time-averaged signals for Lys-  
399 66 and other Lys residues in H<sub>2</sub>O-D<sub>2</sub>O (1:1) appeared exactly in the middle of the spectra observed  
400 in H<sub>2</sub>O and D<sub>2</sub>O (Fig. 5a, c), the fractional factors for the isotopomers are nearly identical, as  
401 statistically random distributions.

#### 402 **4 Conclusions**

403 In this article, we have shown that comprehensive NMR information can be obtained by the  
404 cutting-edge isotope-aided NMR technologies for the Lys side chain moieties, comprising a long  
405 *hydrophobic* methylene chain and a *hydrophilic* ζ-amino group, to facilitate hitherto unexplored  
406 investigations toward elucidating the *dual* nature of the Lys residues in a protein. The  
407 unambiguously assigned <sup>13</sup>C signals, together with the stereo-specifically assigned prochiral  
408 protons for each of the long consecutive methylene chains, which first became available by the  
409 stereo-array isotope labeling (SAIL) method, provide unprecedented opportunities to examine the  
410 conformational features around the Lys residues in detail. The ionization states of the ζ-amino  
411 groups of Lys residues, which play crucial roles in the biological functions of proteins, could be  
412 readily characterized by the deuterium-induced isotope shifts on the ε-<sup>13</sup>C signals observed by the  
413 1D <sup>13</sup>C-NMR spectroscopy of a protein selectively labeled with [ε-<sup>13</sup>C; ε,ε-D<sub>2</sub>]-Lys. Both methods  
414 should work equally well for larger proteins, for which previous NMR approaches were rarely



415 applicable. Therefore, these methods will contribute toward clarifying the structural and functional  
416 roles of the Lys residues in biologically important proteins.

417

#### 418 **Acknowledgements:**

419 This work was supported by Grants-in-Aid in Innovative Areas (21121002, 26119005) to M.K.,  
420 and also in part by the Kurata Memorial Hitachi Science and Technology Foundation and by a  
421 Grant-in-Aid for Scientific Research (C) (25440018) to M.T.

422

#### 423 **References:**

- 424 André, I., Linse, S., and Mulder, F. A.: Residue-specific pKa determination of lysine and  
425 arginine side chains by indirect  $^{15}\text{N}$  and  $^{13}\text{C}$  NMR spectroscopy: application to apo  
426 calmodulin, *J. Am. Chem. Soc.*, 129, 15805-15813. <https://doi.org/10.1021/ja0721824>,  
427 2007.
- 428 Barbas, C. F. 3rd, Heine, A., Zhong, G., Hoffmann, T., Gramatikova, S., Björnstedt, R., List,  
429 B., Anderson, J., Stura, E. A., Wilson, I. A., and Lerner, R. A.: Immune versus natural  
430 selection: antibody aldolases with enzymic rates but broader scope, *Science*, 278, 2085-  
431 2092. [https://doi: 10.1126/science.278.5346.2085](https://doi:10.1126/science.278.5346.2085), 1997.
- 432 Cavanagh, J., Fairbrother, W. J., Palmer, A. G., Rance, M., and Skelton, J. J.: *Protein NMR*  
433 *Spectroscopy: Principles and Practice*, Academic Press, New York, 2007.
- 434 Chimenti MS, Castañeda CA, Majumdar A, García-Moreno E B. Structural origins of high  
435 apparent dielectric constants experienced by ionizable groups in the hydrophobic core of a  
436 protein. *J. Mol. Biol.*, 405, 361-377, <https://doi:10.1016/j.jmb.2010.10.001>, 2011.
- 437 Clore, G. M., Bax, A., Driscoll, P. C., Wingfield, P. T., and Gronenborn, A. M.: Assignment of  
438 the side-chain  $^1\text{H}$  and  $^{13}\text{C}$  resonances of interleukin-1 beta using double- and triple-  
439 resonance heteronuclear three-dimensional NMR spectroscopy, *Biochemistry*, 29, 8172-  
440 8184, [https://doi: 10.1021/bi00487a027](https://doi:10.1021/bi00487a027), 1990.
- 441 Damblon, C., Raquet, X., Lian, L. Y., Lamotte-Brasseur, J., Fonze, E., Charlier, P., Roberts, G.  
442 C., Frère, J. M.: The catalytic mechanism of beta-lactamases: NMR titration of an active-site  
443 lysine residue of the TEM-1 enzyme, *Proc. Natl. Acad. Sci. USA*, 93, 1747-1752,  
444 [https://doi: 10.1073/pnas.93.5.1747](https://doi:10.1073/pnas.93.5.1747), 1996.



- 445 Dziembowska, T., Hansen, P. E., and Rozwadowski, Z.: Studies based on deuterium isotope  
446 effect on  $^{13}\text{C}$  chemical shifts, *Prog. Nucl. Magn. Reson. Spectrosc.*, 45, 1-29, [https://doi:  
447 10.1016/j.pnmrs.2004.04.001](https://doi.org/10.1016/j.pnmrs.2004.04.001), 2004.
- 448 Farmer, B. T. II, and Venters, R. A.: Assignment of aliphatic side-chain  $^1\text{H}/^{15}\text{N}$  resonances in  
449 perdeuterated proteins, *J. Biomol. NMR*, 7, 59-71, [https://doi: 10.1007/BF00190457](https://doi.org/10.1007/BF00190457). 1996.
- 450 Fitch, C. A., Karp, D. A., Lee, K. K., Stites, W. E., Lattman, E. E., and García-Moreno, E. B.:  
451 Experimental  $\text{pK}(\text{a})$  values of buried residues: analysis with continuum methods and role of  
452 water penetration, *Biophys. J.*, 82, 3289-3304, [https://doi: 10.1016/s0006-3495\(02\)75670-1](https://doi.org/10.1016/s0006-3495(02)75670-1),  
453 2002.
- 454 Gao, G., Prasad, R., Lodwig, S. N., Unkefer, C. J., Beard, W. A., Wilson, S. H., and London, R.  
455 E.: Determination of lysine  $\text{pK}$  values using  $[5-^{13}\text{C}]$ lysine: application to the lyase domain of  
456 DNA Pol beta, *J. Am. Chem. Soc.*, 128, 8104-8105, [https://doi: 10.1021/ja061473u](https://doi.org/10.1021/ja061473u), 2006.
- 457 García-Moreno, B., Dwyer, J. J., Gittis, A. G., Lattman, E. E., Spencer, D. S., and Stites, W. E.:  
458 Experimental measurement of the effective dielectric in the hydrophobic core of a protein,  
459 *Biophys. Chem.*, 64, 211-224. [https://doi.org/10.1016/S0301-4622\(96\)02238-7](https://doi.org/10.1016/S0301-4622(96)02238-7), 1997.
- 460 Hansen, P. E.: Isotope effects on nuclear shielding, *Annu. Rep. NMR Spectrosc.*, 15, 105-234,  
461 1983.
- 462 Harris, T. K., and Turner, G. J.: Structural basis of perturbed  $\text{pK}_\text{a}$  values of catalytic groups in  
463 enzyme active sites, *IUBMB Life*, 53, 85-98, [https://doi: 10.1080/15216540211468](https://doi.org/10.1080/15216540211468), 2002.
- 464 Highbarger, L. A., Gerlt, J. A., and Kenyon, G. L.: Mechanism of the reaction catalyzed by  
465 acetoacetate decarboxylase. Importance of lysine 116 in determining the  $\text{pK}_\text{a}$  of active-site  
466 lysine 115, *Biochemistry*, 35, 41-46. [https://doi: 10.1021/bi9518306](https://doi.org/10.1021/bi9518306), 1996.
- 467 Iwahara, J., Jung, Y. S., and Clore, G. M.: Heteronuclear NMR spectroscopy for lysine  $\text{NH}_3$  groups  
468 in proteins: unique effect of water exchange on  $^{15}\text{N}$  transverse relaxation, *J. Am. Chem. Soc.*,  
469 129, 2971-2980. [https://doi: 10.1021/ja0683436](https://doi.org/10.1021/ja0683436), 2007.
- 470 Kainosho, M., and Tsuji, T. Assignment of the three methionyl carbonyl carbon resonances in  
471 *Streptomyces subtilisin* inhibitor by a carbon-13 and nitrogen-15 double-labeling technique.  
472 A new strategy for structural studies of proteins in solution, *Biochemistry*, 21, 6273-6279.  
473 [https://doi: 10.1021/bi00267a036](https://doi.org/10.1021/bi00267a036), 1982.
- 474 Kainosho, M., Torizawa, T., Iwashita, Y., Terauchi, T., Ono, A. M., and Güntert, P.: Optimal



- 475 isotope labelling for NMR protein structure determinations, *Nature*, 440, 52–57, [https://doi:](https://doi.org/10.1038/nature04525)  
476 10.1038/nature04525, 2006.
- 477 Kesvatera, T., Jönsson, B., Thulin, E., and Linse, S.: Measurement and modelling of sequence-  
478 specific pKa values of lysine residues in Calbindin D9k. *J. Mol. Biol.*, 259, 828-839,  
479 <https://doi.org/10.1006/jmbi.1996.0361>, 1996.
- 480 Liepinsh, E., Otting, G., and Wüthrich, K.: NMR spectroscopy of hydroxyl protons in aqueous  
481 solutions of peptides and proteins, *J. Biomol. NMR*, 2, 447-465, [https://doi:](https://doi.org/10.1007/BF02192808)  
482 10.1007/BF02192808, 1992.
- 483 Liepinsh, E., and Otting, G.: Proton exchange rates from amino acid side chains-implications for  
484 image contrast, *Magn. Reson. Med.*, 35, 30-42, [https://doi: 10.1002/mrm.1910350106](https://doi.org/10.1002/mrm.1910350106), 1996.
- 485 Markley, J. L., Bax, A., Arata, Y., Hilbers, C. W., Kaptein, R., Sykes, B. D., Wright, P. E.,  
486 Wüthrich, K.: Recommendations for the presentation of NMR structures of proteins and  
487 nucleic acids, *Eur. J. Biochem.*, 256, 1-15, [https://doi.10.1046/j.1432-1327.1998.2560001.x](https://doi.org/10.1046/j.1432-1327.1998.2560001.x),  
488 1998.
- 489 Markley, J. L., and Kainosho, M.: Stable isotope labeling and resonance assignments in larger  
490 proteins. in *NMR of Macromolecules*, Oxford University Press, 101-152, 1993.
- 491 Otting, G., and Wüthrich, K.: Studies of protein hydration in aqueous solution by direct NMR  
492 observation of individual protein-bound water molecules, *J. Am. Chem. Soc.*, 111, 1871-1875,  
493 <https://doi.org/10.1021/ja00187a050>, 1989.
- 494 Otting, G., Liepinsh, E., and Wüthrich, K.: Proton exchange with internal water molecules in the  
495 protein BPTI in aqueous solution, *J. Am. Chem. Soc.*, 113, 4363-4364, [https://](https://doi.org/10.1021/ja00011a068)  
496 [doi.org/10.1021/ja00011a068](https://doi.org/10.1021/ja00011a068), 1991.
- 497 Poon, D. K., Schubert, M., Au, J., Okon, M., Withers, S. G., and McIntosh, L. P.: Unambiguous  
498 determination of the ionization state of a glycoside hydrolase active site lysine by  $^1\text{H}$ - $^{15}\text{N}$   
499 heteronuclear correlation spectroscopy, *J. Am. Chem. Soc.*, 128, 15388-15389, [https://doi:](https://doi.org/10.1021/ja065766z)  
500 10.1021/ja065766z, 2006.
- 501 Segawa T., Kateb F., Duma L., Bodenhausen G., Pelupessy P.: (2008) Exchange rate constants of  
502 invisible protons in proteins determined by NMR spectroscopy. *ChemBioChem*, 9, 537-542,  
503 [https://doi:10.1002/cbic.200700600](https://doi.org/10.1002/cbic.200700600), 2008.
- 504 Stites, W. E., Gittis, A. G., Lattman, E. E., and Shortle, D.: In a staphylococcal nuclease mutant



505 the side-chain of a lysine replacing valine 66 is fully buried in the hydrophobic core, *J. Mol.*  
506 *Biol.*, 221, 7-14, [https://doi: 10.1016/0022-2836\(91\)80195-z](https://doi.org/10.1016/0022-2836(91)80195-z), 1991.

507 Takayama, Y., Castañeda, C. A., Chimenti, M., García-Moreno, B., and Iwahara, J.: Direct  
508 evidence for deprotonation of a lysine side chain buried in the hydrophobic core of a protein,  
509 *J. Am. Chem. Soc.*, 130, 6714-6715, [https://doi: 10.1021/ja801731g](https://doi.org/10.1021/ja801731g), 2008.

510 Takeda, M., Jee, J., Ono, A. M., Terauchi, T., and Kainosho, M.: Hydrogen exchange rate of  
511 tyrosine hydroxyl groups in proteins as studied by the deuterium isotope effect on C $\zeta$  chemical  
512 shifts, *J. Am. Chem. Soc.*, 131, 18556-18562, [https:// doi: 10.1021/ja907911y](https://doi.org/10.1021/ja907911y), 2009.

513 Takeda, M., Jee, J., Terauchi, T., and Kainosho, M.: Detection of the sulfhydryl groups in proteins  
514 with slow hydrogen exchange rates and determination of their proton/deuteron fractionation  
515 factors using the deuterium-induced effects on the  $^{13}\text{C}\beta$  NMR signals, *J. Am. Chem. Soc.*, 132,  
516 6254-6260, [https://doi: 10.1021/ja101205j](https://doi.org/10.1021/ja101205j), 2010.

517 Takeda, M., Jee, J., Ono, A. M., Terauchi, T., and Kainosho, M.: Hydrogen exchange study on the  
518 hydroxyl groups of Serine and Threonine residues in proteins and structure refinement using  
519 NOE restraints with polar side-chain groups, *J. Am. Chem. Soc.*, 133, 17420-17427,  
520 [https://doi: 10.1021/ja206799v](https://doi.org/10.1021/ja206799v), 2011.

521 Takeda, M., Miyanoiri, Y., Terauchi, T., Yang, C.-J., and Kainosho, M.: Use of H/D isotope effects  
522 to gather information about hydrogen bonding and hydrogen exchange rates, *J. Magn. Reson.*,  
523 241, 148-154, [https://doi: 10.1016/j.jmr.2013.10.001](https://doi.org/10.1016/j.jmr.2013.10.001), 2014.

524 Terauchi, T., Kamikawai, T., Vinogradov, M. G., Starodubtseva, E. V., Takeda, M., and Kainosho,  
525 M.: Synthesis of stereoarray isotope labeled (SAIL) lysine via the "head-to-tail" conversion  
526 of SAIL glutamic acid, *Org. Lett.*, 13, 161-163, [https:// doi: 10.1021/ol1026766](https://doi.org/10.1021/ol1026766), 2011.

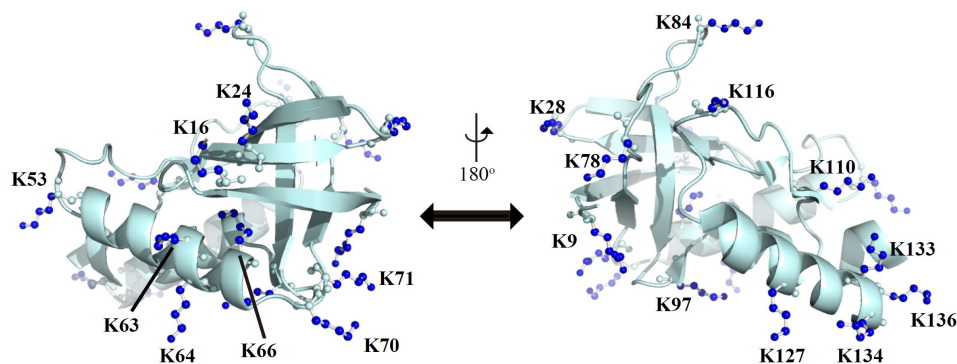
527





528  
529

## Appendices

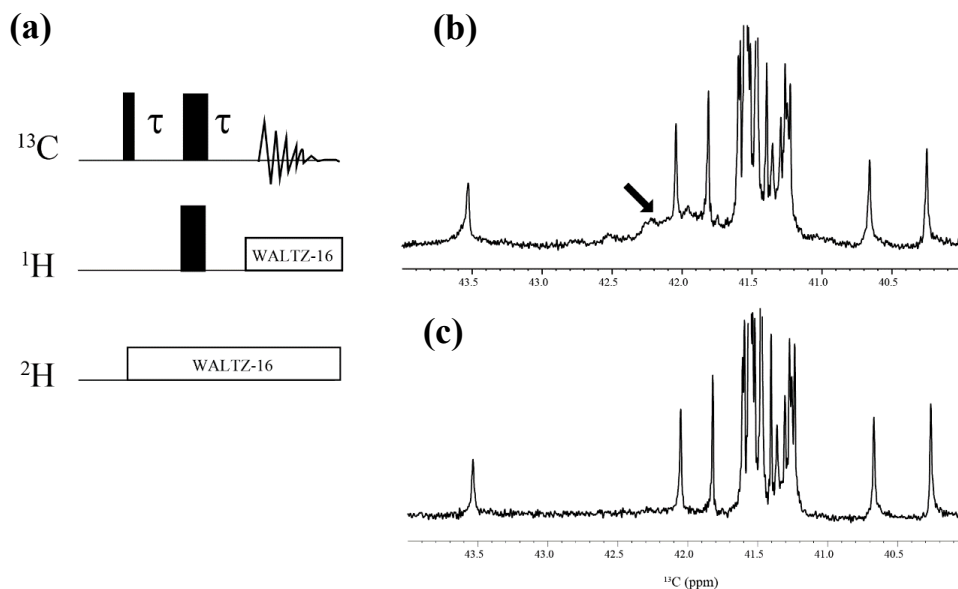


530  
531  
532  
533  
534  
535  
536  
537  
538  
539  
540

**Figure A1: Distribution of the Lys residues in the crystalline structure of the  $\Delta$ +PHS/V66K variant of SNase (PDB#: 3HZX).** All of the side-chain moieties of the Lys residues, which are shown by the ball-and-stick model in blue, exist on the protein surface, except for the Lys-66 (K66). This engineered residue is locked in the protein interior that is originally occupied by the Val sidechain in the wild-type protein. Two Lys residues, K5 and K6, were not visible in the X-ray analysis of the SNase complexed with calcium and thymidine 3',5'-diphosphate and thus it may be slightly different from that in the free state. The figure was created using the Pymol 2.4 software.



541



542

543

544 **Figure A2:  $\{^1\text{H}, ^2\text{D}\}$ -1D  $^{13}\text{C}$  NMR spectra for the SNase variant selectively labeled with  $[\epsilon$ -**

545  $^{13}\text{C}; \epsilon, \epsilon\text{-D}_2\text{]-Lys}$ . The 125.7 MHz  $^{13}\text{C}$  NMR spectra were measured at 25 °C on a Bruker Avance 500 spectrometer

546 equipped with a  $^{13}\text{C}$ -observing DCH cryogenic probe. The broad background signals observed in the spectrum (b),

547 indicated by a thick arrow, are due to the natural abundant  $^{13}\text{C}$  atoms bound to proton(s), which are readily filtered out

548 to give the spectrum (c), by using the pulse scheme shown in (a). The narrow and wide bars in the scheme represent

549 90 and 180 ° rectangular pulses, respectively, and are applied along the x-axis at  $\tau = 1.7$  ms, which corresponds to  $1/4$

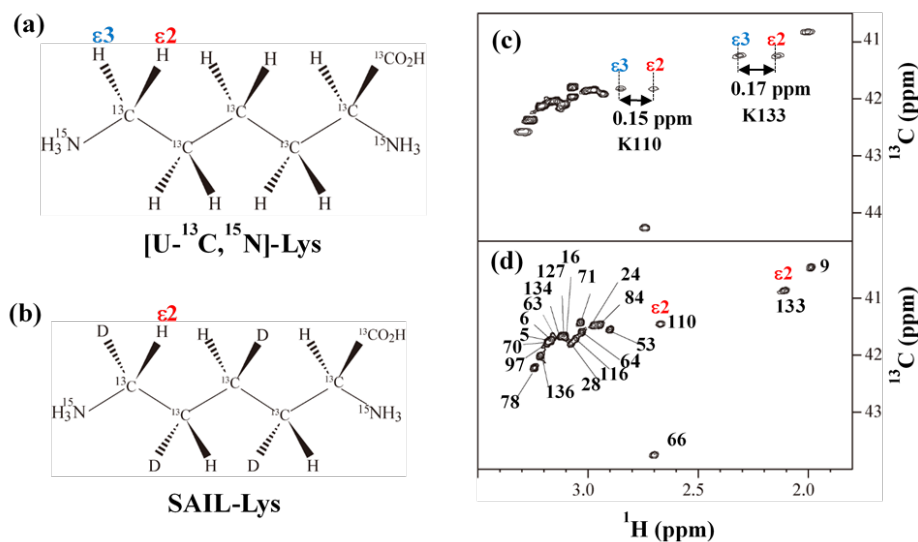
550  $^1J_{\text{CH}}$ . The SNase variant was dissolved in 100 %  $\text{D}_2\text{O}$  buffer, containing 20 mM sodium phosphate and 100 mM

551 potassium chloride at pH 8.0.

552



553



554

555

556

557

558

559

560

561

562

563

564

565

**Figure A3: Comparison between the  $^{13}\text{C}^\epsilon$  regions of the 2D  $^1\text{H}$ - $^{13}\text{C}$  constant time (ct-) HSQC spectra obtained for the SNase variant selectively labeled with [U- $^{13}\text{C}$ ,  $^{15}\text{N}$ ]-Lys (a) and [U- $^{13}\text{C}$ ,  $^{15}\text{N}$ ;  $\beta_2, \gamma_2, \delta_2, \epsilon_3$ -D $_4$ ]-Lys, SAIL-Lys (b). Since  $\epsilon$ -carbons for the [U- $^{13}\text{C}$ ,  $^{15}\text{N}$ ]-Lys residues are attached to the two prochiral protons,  $^1\text{H}^{\epsilon_2}$  and  $^1\text{H}^{\epsilon_3}$ , a pairwise correlation signals, namely  $^1\text{H}^{\epsilon_2}$ - $^{13}\text{C}^\epsilon$  and  $^1\text{H}^{\epsilon_3}$ - $^{13}\text{C}^\epsilon$ , can be observed for each of the  $\epsilon$ -carbons (c). However, considerable large chemical shift difference between the prochiral  $\epsilon$ -methylene protons were observed only for K110 ( $\Delta\delta$ , 0.15 ppm) and for K133 ( $\Delta\delta$ , 0.17 ppm), and the other 19 Lys residues showed the differences less than  $\sim 0.05$  ppm. On the other hand,  $\epsilon$ -carbons for the SAIL-Lys residues are attached only to the  $\epsilon_2$ -protons, all of the correlation signals are automatically assigned to  $^1\text{H}^{\epsilon_2}$  (d).  $\text{C}^\epsilon$  peaks are labeled with their assignment. The spectra were measured at 30 °C on an Avance 600 spectrometer equipped with a TXI cryogenic probe.**



566

|                  | $\chi^1$ | $\chi^2$ | $\chi^3$ | $\chi^4$ |
|------------------|----------|----------|----------|----------|
| <b>K5</b>        | n.d.     | n.d.     | n.d.     | n.d.     |
| <b>K6</b>        | n.d.     | n.d.     | n.d.     | n.d.     |
| <b>K9 Form A</b> | -73.2    | 169.1    | -166.9   | -174.9   |
| <b>Form B</b>    | -78.3    | 170.6    | -152.8   | 44.4     |
| <b>K16</b>       | -171.4   | 176.7    | 32.1     | -126.5   |
| <b>K24</b>       | -169.8   | 156.9    | 146.4    | 171.0    |
| <b>K28</b>       | -79.7    | 176.9    | 161.0    | 148.7    |
| <b>K53</b>       | -171.1   | 164.4    | -164.3   | 163.7    |
| <b>K63</b>       | -179.5   | -172.2   | 159.8    | 73.3     |
| <b>K64</b>       | 164.1    | 178.5    | 174.2    | 165.5    |
| <b>K66</b>       | -102.1   | 107.6    | 81.2     | -72.5    |
| <b>K70</b>       | 81.6     | 134.6    | 171,2    | 77.7     |
| <b>K71</b>       | 175.5    | 164.1    | 140.9    | -157.9   |
| <b>K78</b>       | -69.0    | -72.3    | -173.5   | -143.5   |
| <b>K84</b>       | 65.1     | -166.2   | 166.3    | 160.5    |
| <b>K97</b>       | 175.0    | 175.8    | -155.4   | -144.4   |
| <b>K110</b>      | -83.0    | 169.8    | -179.7   | 177.3    |
| <b>K116</b>      | -148.1   | 133.9    | 98.7     | -164.8   |
| <b>K127</b>      | 168.3    | 65.8     | 163.8    | -67.4    |
| <b>K133</b>      | 171.3    | 156.1    | 17.8     | -178.6   |
| <b>K134</b>      | -134.0   | 155.1    | -71.1    | 126.0    |
| <b>K136</b>      | -67.8    | -112.0   | -142.6   | -50.4    |

567

568 **Table A1: List of the dihedral angles ( $\chi^1, \chi^2, \chi^3, \chi^4$ ) in the crystalline state (PDB #3HZX).**